مجلة دراسات الخليج والجزيرة العربية

مجلة علمية فصلية محكمة تصدر عن مجلس النشر العلمي - جامعة الكويت
صدر العدد الأول منها في يناير عام 1975م

رئيس التحرير

أ. د. بدر عمر العمر

ترحب المجلة بنشر البحوث والدراسات العلمية المتعلقة بشؤون منطقة الخليج والجزيرة العربية في مختلف علوم البحث والدراسة .

ومن أبوابها

- البحوث العربية.
- البحوث الإنجليزية.
- عرض الكتب ومراجعتها.
- البيبليوجرافيا العربية.
- ملخصات الرسائل الجامعية: ماجستير - دكتوراه.
- التقارير: مؤتمرات - ندوات

الاشتراكات

ترسل قيمة الاشتراك مقدماً بشيك لأمر - جامعة الكويت
مسحوب على أحد المصارف الكويتية

داخل دولة الكويت : للأفراد : 3 دنانير - للمؤسسات : 15 ديناراً
الدول العربية : للأفراد : 4 دنانير - للمؤسسات : 15 ديناراً
الدول الغير عربية : للأفراد : 4 دنانير - للمؤسسات : 15 ديناراً

توجه جميع المراسلات باسم رئيس تحرير مجلة دراسات الخليج والجزيرة العربية

Tel.: (+965) 24833215 - 24984066 - 24984067 Fax: (+965) 24833705 P.O. Box 17073 Al-Khaldiah, 72451 Kuwait
www.pubcouncil.kuniv.edu.kw/jgaps E - mail : jgaps@ku.edu.kw
www.ku.edu.kw

Journal of Engg. Research Vol. 2 - (2) June 2014 pp. 155 - 181

النموذج الامثل لأنظمة الكراسي الدوارة المتعددة

عبد العظيم فلاح وعماد خورشيد

قسم الهندسة الميكانيكية جامعة الكويت، صندوق بريد 5969 الصفاة، 13060 الكويت

الخلاصة

تعرض هذه الورقة نموذج رياضي مع نظام تحديد المتغيرات لأنظمة الكراسي المرنة المتعددة المرتبطة بالأقراص الدوارة. وقد تم تحديد الاهتزازات غير المتزنة لنظام الكراسي من خلال التحكم عمليا بدقة الاحمال الساكنة. وتبين عند مقارنة نظام المحاكاة لنظام الكراسي الدوارة عمليا مع البيانات العملية المخبرية ان هناك فروقات واضحة بين البيانات بسبب الاخطاء في تقدير المتغيرات للنموذج الرياضي لنظام الكراسي الدوارة وخاصه التي تتعلق بمتغيرات الصلابة والتخميد. ولزيادة دقة النموذج الرياضي وتقليل الفروقات فقد استخدمت طرق التوقع الامثل لهذه المتغيرات. من إحدى هذه الطرق هي طريقة البحث النمطي لحل هذه المسألة بطريقه عكسية. وباستخدام هذه الطريقة تم تقليل الفروقات بين نظام المحاكاة للكراسي الدوارة مع البيانات العملية المختبرية وخاصه بعد استخدام طرق اخرى مسانده (مثل الشبكات العصبية وطرق أسطح الاستجابة) لتطوير تقدير المتغيرات بحيث قلت جميع الفروقات بالنتائج النهائية للنموذج الرياضي وفي حدود النسب ما بين 9 % إلى 18 %.

Optimum modeling of a flexible multi-bearing rotor system

A. H. FALAH* AND E. A. KHORSHID

*Mechanical Engineering Department, College of Engineering and Petroleum, Kuwait University, P.O. Box 5969 Safat, 13060 KUWAIT

* Corresponding Author: abdulazim.falah@gmail.com

Abstract

Modeling and system identification on flexible multi-bearing rotors with two-concentrated disks are presented in this study. Both rotor unbalance vibration responses through critical speed were experimentally obtained through accurate control of journal bearing static load. Vibration simulations of this laboratory rotor-bearing system were performed as a linear system. The simulation predicted that critical speeds were higher than the experimental ones. These differences strongly occurred because of errors in estimating journal bearing damping and stiffness coefficients. Estimated journal bearing coefficients were carried out by using optimization methods to enhance the model prediction capabilities to the actual test results. The pattern search method was used to solve an inverse problem for the global parameters. A good agreement, in terms of instability threshold speeds and system responses, was found between the experimental results and the optimized model. Both the Response Surface method and the Neural Network method were used to build a Metamodel for predicting the system coefficients. For all tested static loads, the predicted error of the original model was in the range of 9% - 18%.

Keywords: Global optimization; neural network; metamodeling; rotor-bearing systems; system identification.

TOMENCLATURE

L/D	Length/diameter ratio of journal bearing
$c_{xx}^{(1)}$, $c_{yy}^{(1)}$, $c_{xx}^{(3)}$, and $c_{yy}^{(3)}$	Disk air-gap damping coefficients at each balancer
$c_{xx}^{(2)}$, $c_{xy}^{(2)}$, $c_{xy}^{(2)}$, and $c_{yy}^{(2)}$	Damping coefficients for the journal bearing
$k_{xx}^{(1)}$, $k_{yy}^{(1)}$, $k_{xx}^{(3)}$, and $k_{yy}^{(3)}$	Disk air-gap stiffness coefficients at each balancer
$k_{xx}^{(2)}$, $k_{xy}^{(2)}$, $k_{xy}^{(2)}$, and $k_{yy}^{(2)}$	Stiffness coefficients for the journal bearing
$m_1 \cdot r$ and $m_2 \cdot r$	The unbalances at disk 1 and disk 2 respectively

$\underline{X}$ and $\overline{X}$	The lower and the upper bounds of the unknown parameter X.
C	Damping matrix
E	Modulus of elasticity
G	Gyroscopic matrix
I	Moment of inertia
I_p	Polar inertia
K	Stiffness matrix
L_i	Length of each segment
M	Mass matrix of the system
M^d	Disk mass matrix
Mc	Consistent mass matrix
R	Vector of unbalance forces
$R1_{exp}$ and $R2_{exp}$	Experimental maximum displacements of rotors 1 and 2
$R1_{theo}$ and $R2_{theo}$	Theoretical maximum displacements of rotors 1 and 2
V	Potential energy
w	Static load
X_j	Vector of the stiffness and damping coefficients of the journal bearing
z	Vector of generalized coordinates
Ω	Rotor speed

INTRODUCTION

In many industrial applications (turbines, pumps, fans, etc.), the combined demand for high power and speed with continuous operation is increasingly important. The prediction and control of the dynamics behavior (unbalance response, critical speeds and instability) remains an essential issue in the design and analysis of rotating machinery. Parameter identification is required to reduce the difference between experimental measurements and analytical predictions. Identification of the journal bearing hydrodynamic force coefficient is an important step towards the accurate prediction of fluid flow and dynamic response of rotor-bearing systems.

Any theoretical determination of the journal bearing stiffness and damping coefficients is subjected to considerable uncertainty because of the inherent imperfection in any actual bearing's geometrical misalignment, non-uniform fluid viscosity, rotor cracks and hydrodynamic instability. All these imperfections result in inaccurate values of stiffness and damping coefficients of journal bearings. Bearing coefficients calculation using the Sommerfeld number have resulted in large discrepancy in simulating a rotor-bearing system. Estimating journal bearing coefficients has been

carried out by several researchers in the past. One of these methods is the impact impedance, which depends on converting the vibrating response to frequency-dependent transfer functions, to measure the stiffness and damping coefficients of journal bearings (Nordmann & Schollhorn, 1981). Estimating the linearized fluid-film coefficients of two journal bearings from the out of balance responses, where the rigid shaft was conducted by exciting the systems with a known unbalance force (Tieu & Qiu, 1994). The measurements were taken in the time domain and FFT in conjunction with resampling to simplify the data acquisition process and minimize noise effects. Factors other than the unbalanced load could effect on the estimation of the parameters. These are geometry parameters such as the rotary inertia, the gyroscopic inertia, the shear deformation of shaft, and the geometric asymmetry of shaft (Dakel *et al.*, 2014). Moreover, the effect of groove geometry, groove location, supply pressure and bearing geometry were considered in model development of the two journal bearings model (Zengeya & Gadala, 2012).

In addition, new method for identifying the stiffness and the damping coefficients of the journal bearing are conducted by updating the eccentricity ratio at a spin speed (Chouksey *et al.*, 2014). This work is mainly done based on Inverse Eigen-sensitivity method. Eccentricity ratio and coefficient of shaft material damping are updated in this process to identify bearing model and internal friction force at any speed. Updating of eccentricity ratio to identify journal bearing coefficients is considered a new approach that eliminates the need to update eight bearing coefficients per bearing and hence helps in effective parameterization in the model updating process. Another technique for estimating non-linear stiffness of rolling element bearings is performed by processing random response signals that were picked up from caps of rotor bearing systems (Tiwari & Vyas, 1995). The advantage of this technique is the negligence of excitation force measurement and the straight determination of the random response signal. Identified oil film coefficients of large journal bearings on a full scale journal bearing testing has been done by many researchers (Jiang *et al.*, 1997; Yang & Lin, 2009). They applied a nonlinear optimization algorithm to identify stiffness and damping coefficients. However, since the test conditions of the experiments were limited, the results were unsatisfactory (Jiang *et al.*, 1997). The non-linear stiffness parameters of rolling elements bearing were identified by using random response of flexible rotor-bearing caps (Tiwari & Vyas, 1997). This method did not account for shaft flexibility and thus the analysis was only of a single-degree-freedom. The fluid film bearing coefficients were obtained from measurements of bearing dynamic response due to periodic forces applied by shakers (Andres & Santiago, 2004; Andres & Santiago, 2005). Journal bearing force coefficients under high dynamics loading was subsequently determined. Optimization methods are frequently used for solving

inverse problems such as parameter estimation (Rosa *et al.*, 1997; Nicoletti, 2013). The variation of nonlinear stiffness and damping coefficients of journal bearing relative to equilibrium position was investigated (Sawicki & Rao, 2004). The dynamic pressure gradient was considered as a first order perturbation of static pressure. Higher order pressure gradients for displacement and velocity perturbations were also used to obtain nonlinear dynamic coefficients. A numerical identification of nonlinear fluid film bearing parameters considering large journal orbital motion was proposed (Meruane, & Pascual, 2008). Stiffness and damping coefficients were obtained using Taylor series expansion of the bearing fluid film forces in terms of both perturbation displacements and velocities.

Other researchers use effective method based on Kriging surrogate model and evolutionary algorithm to identify the bearing parameters and unbalance information in rotor-bearing system (Han *et al.*, 2013). The developed algorithm has been tested with numerical example and experimental application, where it effectively reduces the computational expense of parameter identification.

Based on a review of the current published research, the purpose of this study was to calculate the journal bearing coefficients using analytical and experimental approaches with the help of the pattern search optimization technique. The ultimate objective of this study was to investigate the influence of bearings and supports upon the entire rotor dynamics. Numerical examples and experimental results were used to demonstrate new approach capabilities. The enhanced model with the newly identified parameters accurately predicts the dynamic responses of the entire rotor-bearing system under different static loads.

MATHEMATICAL MODEL

The model used to simulate the entire rotor system contains 12 generalized coordinates (DOFs), two angular displacements and two radial displacements at each of the three locations shown in Figure 1:

$$z = [x_1, y_1, \theta_1^x, \theta_1^y, x_2, y_2, \theta_2^x, \theta_2^y, x_3, y_3, \theta_3^x, \theta_3^y]^T \quad (1)$$

where x_i, y_i are the radial displacements and θ_i^x, θ_i^y are the angular displacements of the three locations of i=1, 2 and 3.

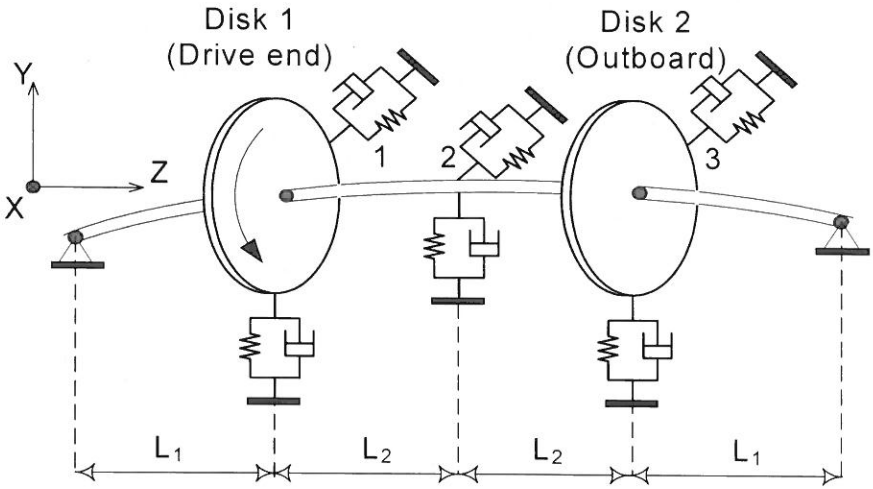

Fig. 1. 12-DOF test rig model using mass stations.

The complete model is shown in Figure 1. However, the third disk in the middle of the shaft, where the journal bearing is located, is actually not present in the test rig. This "virtual" disk is just used to obtain the shaft's stiffness matrix using linear beam theory. The shaft was subdivided into four beams that are classified into two different types of the same length. The masses were divided and concentrated at three stations. In contrast to stations 1 and 3, station 2 has no polar inertia at the disk and is just assumed to contribute to the stiffness matrix, (Figure 2). Naturally, the mass and transverse inertia at station 2 is smaller than at stations 1 and 3.

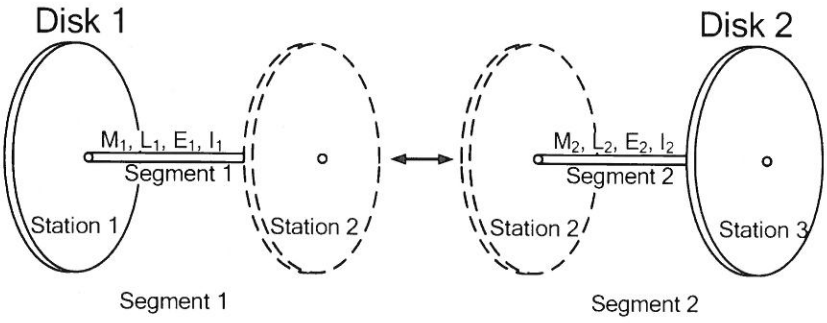

Fig. 2. Subdivided part of the model used for the derivation of the stiffness matrix.

The general equations of motion for the model with 12 degrees are:

$$\mathbf{M}\cdot\ddot{z}+(\mathbf{C}+\mathbf{G})\cdot\dot{z}+\mathbf{K}\cdot z=R \tag{2}$$

where z: Vector of Generalized Coordinates, M: Mass Matrix, C: Damping Matrix, G: Gyroscopic Matrix, K: Stiffness Matrix and R: Vector of Unbalance Forces. Note that the sizes of the matrices are $\{\mathbf{M},\mathbf{C},\mathbf{G},\mathbf{K}\}^{12\times12}$, $\{\ddot{z},\dot{z},z,R\}^{12\times1}$.

The shaft element is considered to have a uniform cross section and is subjected to bending moment. A finite element analysis with the approximation shape function (deflection shape function) was used to obtain the element mass matrix. Masses of disks 1 and 2 are lumped at their corresponding stations, namely stations 1 and 3. The complete mass matrix resulting from the addition of the shaft matrix and disk matrix is

$$M_{complete} = M_{shaft} + M_{disk} \tag{3}$$

where Mshaft is a consistent mass matrix (Adams, 2001; Falah, 2002)

The matrix [C] contains the additional outer damping represented by the journal bearing at station 2 and the air gap dampers at disks 1 and 2. $c_{xx}^{(1)}, c_{yy}^{(1)}, c_{xx}^{(3)}$, and $c_{yy}^{(3)}$ are the disk air-gap damping coefficients at each balancer. These parameters are assumed zero at the present study, since they have a minor effect on the response of both rotors. $c_{xx}^{(2)}, c_{xy}^{(2)}, c_{xy}^{(2)}$, and $c_{yy}^{(2)}$ are the damping coefficients of the journal bearing. The gyroscopic moment components that are applied to each disk at stations 1 and 3 are expressed as follows:

$$\begin{aligned} M_{gyro,x} &= -I_p \Omega \dot{\theta}_y \\ M_{gyro,y} &= +I_p \Omega \dot{\theta}_x \end{aligned} \tag{4}$$

where ΩI_p represent the gyroscopic coefficient at the end of disk.

The stiffness resulting from the shaft flexibility is obtained by using the classical linear beam theory (Cook *et al.*, 2001). The problem is thus divided into three parts. The stiffness of the two beams connecting the two disks is calculated (beam type 2). The resulting stiffness beams between the disks and the support are derived. Finally, the additional outer stiffness from each disk and that of the journal bearing coefficients are considered. The additional stiffness matrix $K_{additional}$ has $k_{xx}^{(1)}, k_{yy}^{(1)}, k_{xx}^{(3)}$, and $k_{yy}^{(3)}$ for the disk air-gap stiffness coefficients at each balancer. These coefficients are assumed zero. $k_{xx}^{(2)}, k_{xy}^{(2)}, k_{yx}^{(2)}$, and $k_{yy}^{(2)}$ are the stiffness coefficients for the journal bearing. The complete stiffness matrix is:

$$K = K_{additional} + K_{Shaft} \tag{5}$$

The stiffness and damping coefficients for the cylinder journal bearing are calculated initially, considering non-dimensional damping coefficients of the cylindrical journal bearing at different Sommerfeld numbers and for a Length/diameter ratio (L/D) equals to ½. The unbalance forces are introduced by two static unbalances that can be set independently at stations of the two disks. The unbalance forces are effective in the

lateral directions at these stations (in the x-y plane) and are given by:

$$R = \Omega^2 \cdot \begin{bmatrix} m_1 \cdot r \cdot \cos(\Omega t + \phi_1) \\ m_1 \cdot r \cdot \sin(\Omega t + \phi_1) \\ 0 \\ 0 \\ 0 \\ 0 \\ 0 \\ 0 \\ m_2 \cdot r \cdot \cos(\Omega t + \phi_2) \\ m_2 \cdot r \cdot \sin(\Omega t + \phi_2) \\ 0 \\ 0 \end{bmatrix} \tag{6}$$

Here, $m_1 r$ and $m_2 r$ are the unbalances at disk 1 and 2 respectively, m is the unbalance mass and r is the distance (Figure 3).

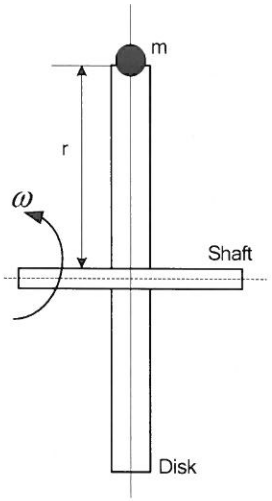

Fig. 3. Static rotor disk unbalance.

In Equation (6), Ω is the rotor speed ϕ_1 and ϕ_2 are the phase angles between the unbalance at each disk, respectively.

PARAMETER ESTIMATION PROBLEM STATEMENTS

In the parameter estimation technique, the unknown variables are the parameters of the mathematical model. This step was conducted after completing the entire required elements in the mathematical model of the rotor-bearing system. The problem formulation of the parameter estimation, or what is defined as an inverse problem, and the solution method are discussed in this section.

The 12 second-order differential equations of motion in Equation (2) were transformed into 24 first order differential equations of the following form

$$\{\dot{y}\}_{24\times1} = A\{y\}_{24\times1} + B \tag{7}$$

where

$$[A] = \begin{bmatrix} [0]_{12\times12} & [I]_{12\times12} \\ -[M]^{-1}_{12\times12} \bullet [K]_{12\times12} & -[M]^{-1}_{12\times12} \bullet [C]_{12\times12} \end{bmatrix}_{24\times24} \tag{8}$$

$$[B] = \begin{bmatrix} [0]_{12\times1} \\ [M]^{-1}_{12\times12} \quad [R]_{12\times1} \end{bmatrix}_{24\times1} \tag{9}$$

$$\{\dot{y}\} = \begin{Bmatrix} \dot{y} \\ \ddot{y} \end{Bmatrix}_{24\times1} \tag{10}$$

$$\{y\} = \begin{Bmatrix} \{y\} \\ \{\dot{y}\} \end{Bmatrix}_{24\times1} \tag{11}$$

where $[I]$ is the identity matrix.

The parameter estimation of journal bearing damping and stiffness coefficients, contained in X, is obtained mathematically by solving the following mathematical programming problem as:

Given: Unbalance force applied on each balancer, oil viscosity, static load, and operating speed

Find: Unknown parameters (damping and stiffness coefficients of the journal bearing)

$$X=\left[c_{xx}^{(2)}, c_{xy}^{(2)}, c_{yx}^{(2)}, c_{yy}^{(2)}, k_{xx}^{(2)}, k_{xy}^{(2)}, k_{yx}^{(2)}, k_{yy}^{(2)}\right]$$

To Minimize:
$$F(X)=\sum_{i=1}^{n}\left(R1_{\text{exp}}-R1_{\text{theo}}\right)_i^2+\sum_{i=1}^{n}\left(R2_{\text{exp}}-R2_{\text{theo}}\right)_i^2 \quad (12)$$

Subject to:
$$\underline{X} \le X \le \overline{X}$$

$R1_{\text{exp}}$ and $R2_{\text{exp}}$ are the experimental maximum displacements of rotors 1 and 2, $R1_{\text{theo}}$ and $R2_{\text{theo}}$ are the theoretical maximum displacements of rotors 1 and 2, i is the index of the input speed Ω and n is the total number of runs. Also, $\underline{X}$ and $\overline{X}$ are the lower and the upper bounds, respectively, of the unknown parameter in the vector $\{X\}$.

This problem is a nonlinear constrained optimization program (NLP). By computational experimentation of the optimization problem in Equation (12), local minima of $\{X\}$ could be found. Finding the global optimum is a great challenge because it requires larger combination numbers of the initial values for the design parameters (Assis & Steffen, 1999). Genetic algorithm, simulated annealing and evolutionary optimization, all belong to the family of global search methods, which are also known as stochastic algorithms (Camargo *et al.*, 2010; Castro, 2013; Lia *et al.*, 2014). Recently, stochastic algorithms have achieved popularity, mainly for their distinguished properties. These are performing global optimizations, requiring no or very low accurate gradient information, using probability rules to guide their searches and being suitable for solving complex real-world problems. Stochastic algorithms achieve the above merits at the expense of requiring more function evaluations compared with conventional optimization algorithms (Goldberg, 1989). In order to find the global solution for the estimated parameters, the pattern search method was selected (Lia *et al.*, 2014). Pattern search is a method for solving optimization problems that does not require any information about the gradient of the objective function ($F(x)$ in Equation (12)). A direct search algorithm searches a set of points around the current point, looking one, where the value of the objective function is lower than

the value at the current point. This is more suitable than the traditional optimization methods that use information about the gradient or higher derivatives to search for an optimal point. The pattern search method can be used to solve problems for which the objective function is not differentiable, or even continuous. This fits the optimization problem in Equation (12) since the objective function is non-differentiable. The non-differentiability occurs because the values of $R1_{theo}$ and $R2_{theo}$ are obtained by solving the set of differential equations described in Equation (2).

GENERAL PROCEDURE FOR ESTIMATING THE COEFFICIENTS

The general procedure for estimating the journal bearing coefficients is shown in Figure 4.

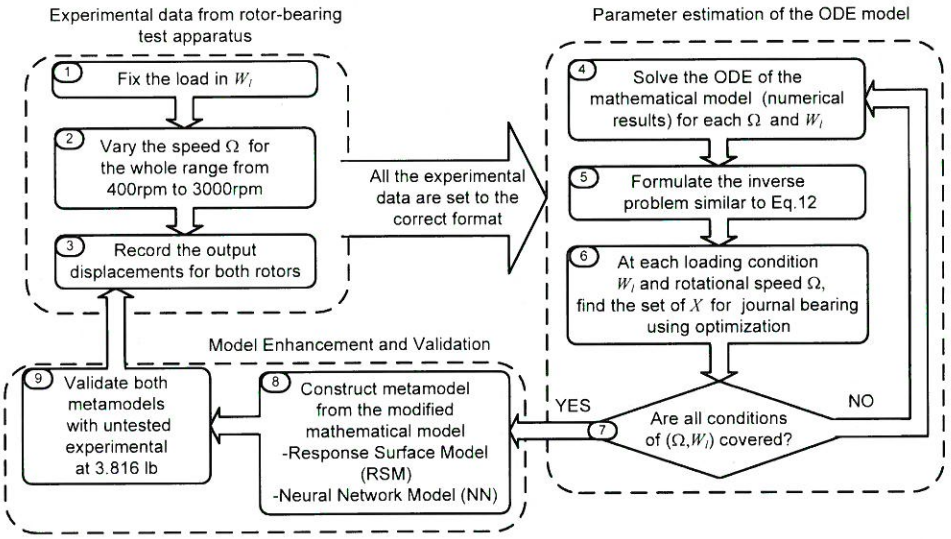

Fig. 4. General procedure for parameter estimation of the journal bearing coefficients using the pattern search method.

The steps of Figure 4 can be explained in details as follows:

Step 1: The experimental data is collected for different loading conditions and various speeds.

Step 2: The four load cases used for parameter estimation are defined in the vector W_i=[0.823 1.32 1.817 2.316] lb. The untrained load, which will be used for testing the model validity, is at 3.816 lb. The speed range for Ω is varied from 400 to 3000 rpm.

Step 3: At each combination of load-speed, the amplitude and the phase angle of balancer 1 and 2 are recorded. The experimental data collection is repeated

for all specified ranges of load-speed combinations. The experimental data is set in the correct format for feeding to the parameter estimation of the ODE mathematical model, *i.e.* in the vectors of $\left(R1_{\exp}, R2_{\exp}\right)$.

Step 4: From step 4 to 6, the aim is to estimate the unknown parameters using the Pattern Search optimization method. At each combined condition of (W_l, Ω), the Nonlinear differential equation is solved numerically using the Runge–Kutta method. This method can be called in MATLAB by function ODE45. The output resulted from this solution (for each loading condition) is the displacement of both rotors of the journal bearings $\left(R1_{\text{theo}}, R2_{\text{theo}}\right)$.

Step 5: Formulate the inverse problem similar to Equation (12). This requires that all the vectors of the experimental and the theoretical data will be of the same length, and the entire upper and lower bounds of the unknown coefficients $\left(\underline{X}, \overline{X}\right)$ are set to be within 30% of the coefficient of the Sommerfeld number.

Step 6: The unknown parameters $X=\left[c_{xx}^{(2)}, c_{xy}^{(2)}, c_{xy}^{(2)}, c_{yy}^{(2)}, k_{xx}^{(2)}, k_{xy}^{(2)}, k_{xy}^{(2)}, k_{yy}^{(2)}\right]$ are estimated using the Pattern search method (Lia *et al.*, 2014). The pattern search algorithm starts with an initial point with a finite function value, followed by a series of iterations, each of which consists of an optional search step and a local poll step. Both steps evaluate points on a carefully constructed mesh in an attempt to find an improved mesh point; *i.e.*, one with a lower objective function value than that of the incumbent. The mesh is constructed as a lattice based on a set of directions that form a positive spanning set (Charles & Dennis, 2004). In the search step, any finite set of mesh points can be evaluated. This allows the user great flexibility in choosing points. If the search step is empty or unsuccessful in finding an improved mesh point, then the poll step is invoked. In this more rigidly defined step, the neighboring mesh points to the current iterate are evaluated. The fact that these neighboring points are constructed by means of positive spanning sets drive the convergence theory for the algorithm. If the search and poll steps are both unsuccessful, then the current incumbent is declared a mesh local optimizer, and the mesh is refined by reducing a single mesh size parameter. If an improved mesh point is found in either step, then the mesh is either retained or coarsened by increasing the mesh size parameter (Torczon, 1997).

Step 7: The loop will continue from step 4 to step 6 until all the loading conditions (w_l, Ω) are covered.

Step 8: This step is to collect the data from the previous parameter estimation step and present them in three-dimensional plots. The Response Surface

Model (RSM) is built for quick estimation of the system's eight unknown parameters at any speed and load condition. The second-order model is

$$x(W_l,\Omega)=a_0+\sum_{i=1}^{N}a_iW_{li}+\sum_{j=1}^{M}a_j\Omega_j+\sum_{i<j}^{N}\sum_{j=2}^{M}a_{ij}W_{li}\,\Omega_j+\sum_{i=1}^{N}a_{ii}W_{li}^{2}+\sum_{j=1}^{M}a_{jj}\Omega_j^2 \quad (13)$$

The model includes, from left to right, an intercept, linear terms, quadratic interaction terms and squared terms. Linear terms alone produce models with response surfaces that are hyperplanes. The addition of interaction terms allows for warping of the hyperplane. Squared terms produce the simplest models in which the response surface has a minimum or maximum, and so an optimal response. The second-order model is widely used in response surface methodology because of its flexibility and its capability to approximate the true response surface. Another reason for using the RSM model is simplicity in estimating the parameters (the a's) in the second-order model using the least squares. The RSM model is conducted in MATLAB using the statistical toolbox.

For comparison reasons, another metamodel is built: the NN model. The objective is to increase the prediction accuracy of the rotor-bearing metamodel especially for untrained input, where such as that of load 3.816 lb. However, to find any new coefficients with different static load or speed, it must solve the inverse problem. The objective of this step is to build a neural network model that can be easily used to estimate the unknown coefficients without going through the complicated details of modeling and optimization. The neural network (NN) modeling technique is suitable for building the metamodel, since it has a great capability for approximating nonlinear input-output relations, and it can quickly calculate the output results of the rotor-bearing coefficients at any static load and rotor speed. The MATLAB Neural Network toolbox is used to build the NN model (Beale *et al.*, 2012). The type of NN models is the Feed Forward Backpropagation network (FFBP). The network, with *two* inputs of the vector $\{\Omega, w\}$ and eight outputs of the parameter's vector is shown in Figure 5 $\left(c_{xx}^{(2)}, c_{xy}^{(2)}, c_{yx}^{(2)}, c_{yy}^{(2)}, k_{xx}^{(2)}, k_{xy}^{(2)}, k_{yx}^{(2)}, k_{yy}^{(2)}\right)$.

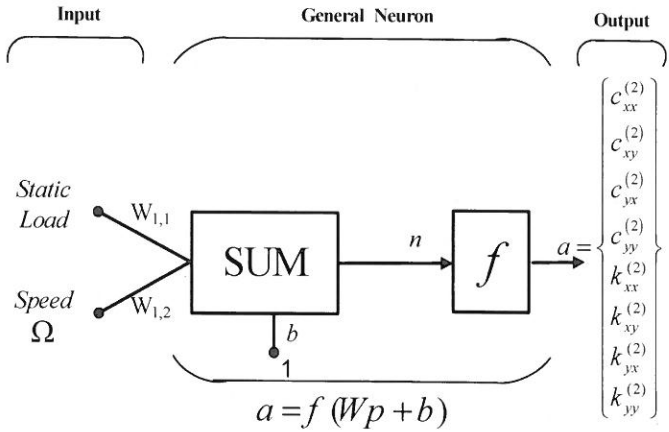

Fig. 5. Backpropagation bases neuron.

EXPERIMENTAL SETUP

The details of the experimental setup used in this study are shown in Figure 6. The test setup consisted of two identical maximum precision duplex angular contact preloaded ball bearings at each end of the shaft. The bearing span was 30 inches (760 mm). The shaft (journal) had a diameter of 0.65 inches (16.5 mm). It was powered by a very thin and flexible quill shaft connected to a small DC motor with an accurate stable speed control of up to 10,000 rpm.

The setup allows for real-time control of two identical rotor balancers. Each rotor contained two internal circumferential stepping motors that could be placed angularly to its eccentric mass, relative to a fixed point on the rotor with 5° stepping increments. The balancer consisted of rotating and stationary components. The stationary part was fixed to the casing of the test rig. Power was passed from the stationary to the rotating balancer ring in the balancer by inducing a magnetic field across an air gap. Thus, no mechanical contact between stationary and rotating components could take place. The real-time balancers were used to place known controlled mass unbalances at their two respective axial locations. More details about the setup can be reviewed in (Adams & Falah, 2004).

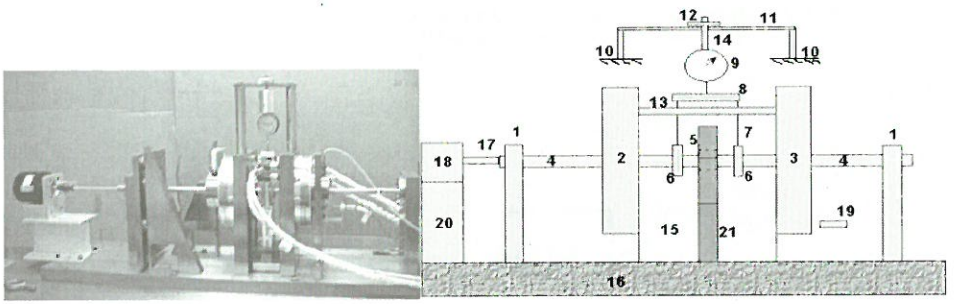

Legend:

1- End bearing
2- Drive end balancer
3- Outboard balancer
4- Shaft
5- Journal bearing
6- Load support
7-Rods
8- Beams
9- Load measurement device
10- Columns
11- Beam
12- Knob
13- Lid
14- Threaded rod
15- Oil tank
16- Table support
17- Quill shaft
18- DC motor
20- Motor support base
19- Key phasor
21- Aluminum base

Fig. 6. Experimental setup.

The length and the diameter of the shaft made it a dynamically and statically flexible one. The high degree of static radial flexibility made it a fairly simple and accurate component to apply a controlled radial static load on its mid-span oil-film journal bearing. Both components are shown in Figure 6 and are labeled "load support" (6). They were actually very narrow (1.6 mm) 180° partial-arc oil-film journal bearings, with relatively large radial clearance. Table 1 outlines the journal bearing parameters. They were used to transmit the controlled radial static load to the statically flexible shaft. These two load-support applicator bearings were dimensioned to operate on extremely thin oil films. Therefore, the effective radial stiffness of them was at least an order-of-magnitude higher than that of any other flexible member.

The nominal bore diameter of the oil-film journal bearing was the same as the shaft and had a nominal radial clearance of 0.008 inches (0.20 mm).

Table 1. Oil-film journal bearing parameters

Bearing active length	8.25 mm (0.325 inches)
Bearing bore diameter	16.5 mm (0.65 inches)
Radial clearance	0.20 mm (0.008 inches)
Static radial load range	2.2 – 17.8 N (0.5 – 4.0 lb.)
Oil dynamic viscosity	550 centipoise (80 micro-reyn)

EXPERIMENTAL PROCEDURE

The entire rotating assembly was first balanced as precisely as possible, using the two Baladyne rotor-based balancers. The remaining residual measured rotor vibration signals were electronically stored for subsequent real-time digital subtraction from their respective rotor total vibration signals. These signals occurred when known additional unbalances were added by operating the Baladyne rotor-mounted balancers in their manual control mode. The rotor speed was then increased incrementally and the amplitude and phase angle for each balancer were recorded at each speed. All control signals and unbalance position data were fed through a magnetic coupler to a local controller driven by a PC. The net rotor vibration signals were then used in direct comparisons with their counterparts obtained from computational simulations under the same running conditions.

RESULTS AND DISCUSSIONS

The test apparatus was mathematically modeled using two different rotor-bearing systems. In the first one, the rotor-bearing mathematical model without the identification technique (defined as the Original Model) was used. In the second model, the unknown parameters of damping and stiffness coefficients were estimated with the pattern search technique and added to the model (defined as the Enhanced Model). The following sections discuss all the numerical findings with the simulation and the parameter estimation techniques.

Errors in the Rotor-bearing Coefficients

Any theoretical determination of the journal bearing stiffness and damping coefficients is subjected to considerable uncertainty because of the inherent imperfection in any actual bearing's geometry, misalignment, non-uniform viscosity, etc., as compared to the assumed computational inputs. All these imperfections resulted in inaccurate values of the stiffness and damping coefficients of the journal bearing. Therefore, these coefficients calculated from the Sommerfeld number (Figures 7 and 8) added large errors in simulating the rotor-bearing system. Figures 7 and 8 are a graphic representation of the estimated coefficients; based on the Sommerfeld number; as a function of load and speed. From these figures, these coefficients have a smooth relation with load and speed with no noise in them. Both Figures show the minimum and the maximum values of the estimated coefficients. Figure 9 shows these large simulated errors for the rotor vibration response of disk 2 as a function of the input speed. These errors are amplified in the speed range from 500 to 1100 rpm and in the unstable region from 2000 to 3000 rpm. Figures 7 and 8 show that if load is increased, then the stiffness and damping coefficients of the journal bearing are increased in an approximately linear pattern.

Therefore, one of the techniques to enhance the mathematical model is to find these coefficients using the proposed system identification technique. The procedure for system identification assumes that these coefficients of the journal bearing, which are $X_j=\left[c_{xx}^{(2)}, c_{xy}^{(2)}, c_{xy}^{(2)}, c_{yy}^{(2)}, k_{xx}^{(2)}, k_{xy}^{(2)}, k_{xy}^{(2)}, k_{yy}^{(2)}\right]$, are both speed and load dependent. This means that at each given load and running speed, the coefficients in X_j are estimated by solving the inverse problem in Equation (12). The next section discusses the procedure for the solution process.

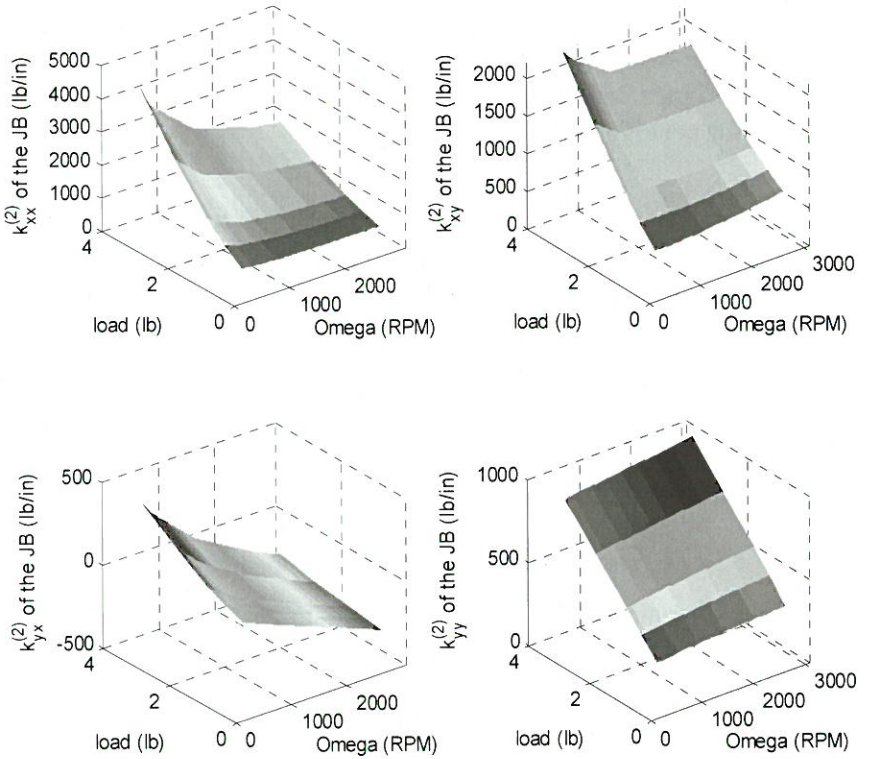

Fig. 7. Journal bearing stiffness coefficients as a function of load and speed obtained from the Sommerfeld number and RSM.

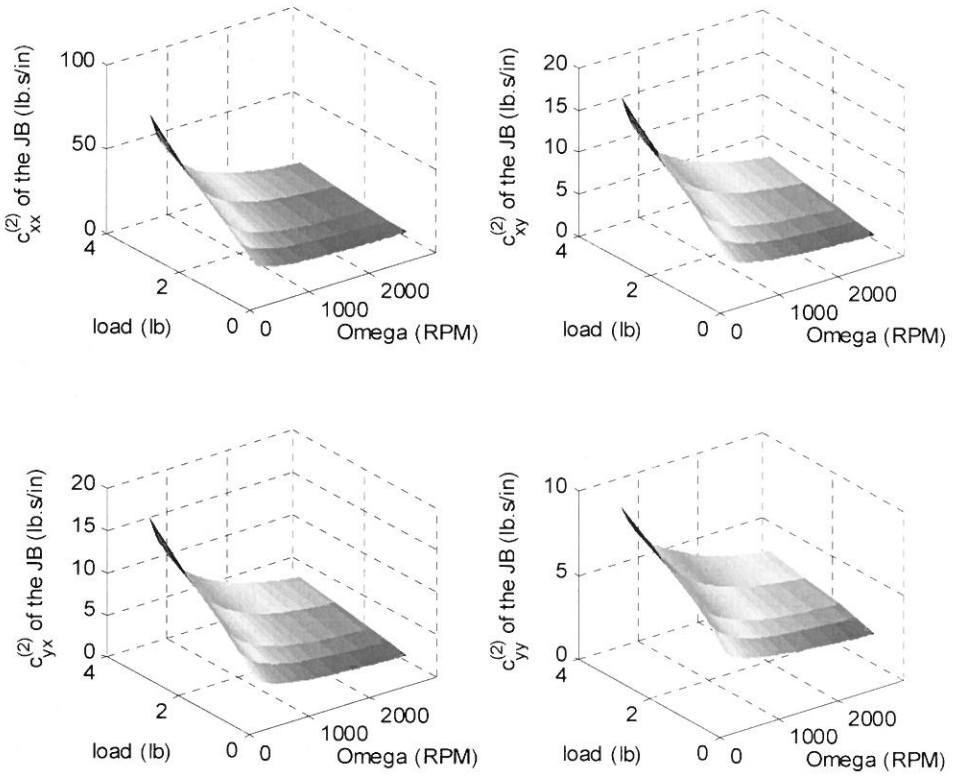

Fig. 8. Journal bearing damping coefficients as a function of load and speed obtained from the Sommerfeld number and RSM.

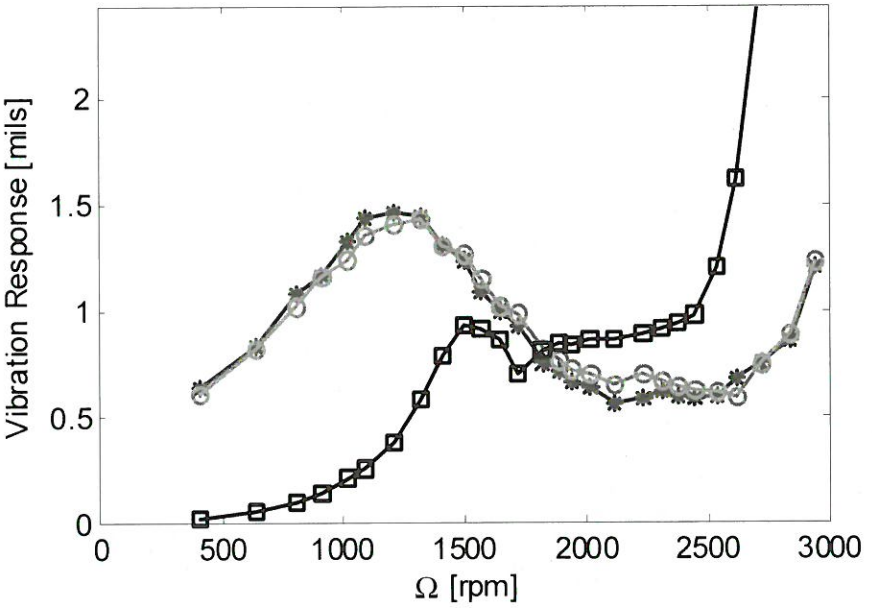

Fig. 9. Rotor vibration synchronous response of disk 2 (displacement) with input load = 10.3 N (2.316 lb) for (—□—) Simulation with system coefficients based on Sommerfeld number. (···✱···) Simulation with system coefficients based on parameter estimation. (—○—) Experimental.

Parameter Estimation of the Unknown Coefficients

As stated before, the estimated parameters are classified in the vector (X_J), which represents the unknown stiffness and damping parameters of the journal bearing. The initial guess for the unknown parameters of group X_J is set to be $X_{Sommerfeld}$, which is the stiffness and damping coefficients from the Sommerfeld number (Figures 7 and 8). For experimental computations, these values of the Sommerfeld number provide good initial guesses for solving the parameter estimation problem for the X_J variables. On the other hand, the unknown parameters for group X_A is set to zero, which represents the case when the disk air-gap model is assumed to have a very small effect on the system dynamics. This was confirmed after several computational experimentations in which it was observed that these air gap parameters have a negligible effect on the model response. Therefore, the air gap parameters are assumed zero. The upper and lower bounds for the X_J parameters are set to ±30% of $X_{Sommerfeld}$ (Kostrzewsky *et al.*, 1997).

At this point, all the required elements to solve the inverse problem of Equation (12) are completed. At each load in W_l and Ω speed, a set of eight unknown parameters will be estimated. Sample iteration for the patterns search method is shown in Figure 10. This figure represents the variation of the objective function versus the iteration

number. Fig. 10b shows the change in grid mesh size as a function of the iteration. Fig. 10c demonstrates the fluctuation of the function evaluation per interval between 7 and 10 evaluations at each iteration. Finally, the optimal solutions, *i.e.* solution for the unknown parameters in Equation (12), are shown in Fig. 10d.

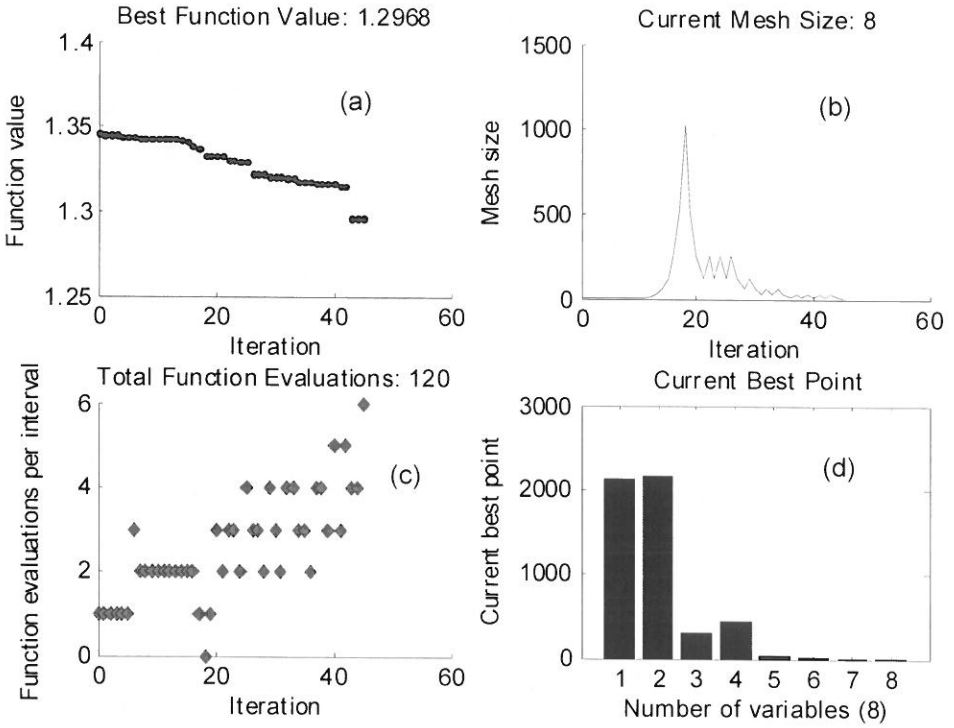

Fig. 10. The variations of (a) function values, (b) mesh size, (c) function evaluations per interval and (d) the final best point in Pattern search method.
Figures a- c are a function of iteration number.

After completing the parameter estimation process for all the static loads in w with the entire range of speeds Ω, the next step was to visualize these results in a three-dimensional plot (Figure 11 and 12). Figure 11 shows the variation of the stiffness coefficient of the journal bearing with respect to static load and speed. Several important observations can be made regarding the data in Figure 11. First, the journal bearing has a lower stiffness in the y-direction $\left(k_{yy}^{(2)}\right)$ than that in the x-direction $\left(k_{xx}^{(2)}\right)$ due to the applied static load in the opposite y-direction (upward). Second, the identified results of the cross stiffness $\left(k_{xy}^{(2)}, k_{yx}^{(2)}\right)$ are of the same order of magnitude as those of the theoretical stiffness measured from non-dimensional stiffness (Figure 7). Third, it is clear that the stiffness coefficient $k_{xy}^{(2)}$ is increased by increasing the static load, whereas the other coupling stiffness coefficient $k_{yx}^{(2)}$ does not vary by the applied static load. Unstable regions between 1500 to 2500 rpm are

observed due to threshold instability, which approximately occurs at about half of the natural frequency.

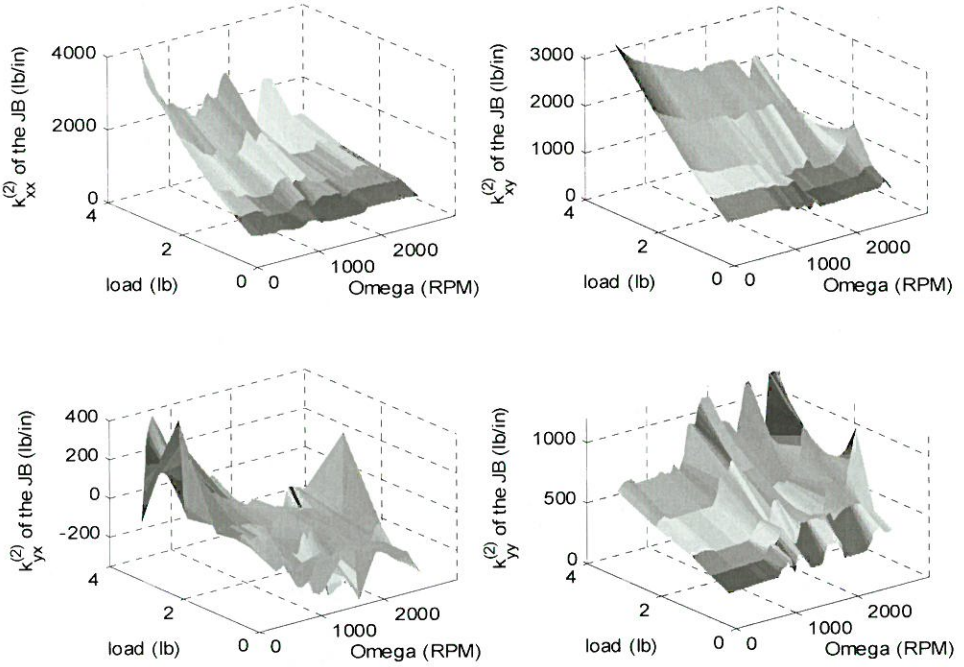

Fig. 11. Estimated journal bearing stiffness coefficients as a function of load and speed based on the Neural Network Model (Metamodel of the theoretical model).

The peaks on the 3D plot of the journal bearing stiffness coefficient may occur due to the errors in the experimental measurements of the rotor responses, which forced the coefficients to accommodate for these errors (Figure 11 and 12). Another reason for these peaks in the unstable region is the existence of many local minimums for the unknown estimated parameters. To minimize the appearance of these peaks, a solution method for global optimal parameter estimation, such as the pattern search algorithm (PS), should be used (Lia *et al.*, 2014). Other methods for local minimum and fast convergence rate, such as the Sequential Quadratic Programming method (SQP) failed during the solution process. They caused the solver of the ordinary differential equation of the dynamic system to crash. This was the main reason the SQP method was replaced by the PS method.

Another observation from Figure 11 is the appearance of an unstable region that occurs in the range of 1500 to 3000 rpm for all load conditions. The unstable region has a great influence on the estimated damping coefficients in X_j. For example, the values of $k_{yy}^{(2)}$ vary severely in this region. Whereas, before and after this unstable

region, the values of $k_{yy}^{(2)}$ have a unified pattern. These estimated damping coefficients also increase in the unstable region to their maximum limit. On the other hand, they converge to their minimum lower bounds outside the unstable range (region), because the rotor-bearing system is under the effect of the threshold instability. The estimated parameters in Figure 12 for the journal bearing damping coefficients show the same trend as that from the Sommerfeld number of Figure 8. However, small variations in the values of $\left\{c_{xx}^{(2)}, c_{xy}^{(2)}, c_{yx}^{(2)}, c_{yy}^{(2)}\right\}$ occur in the range of 2000 to 2800 rpm due to threshold instability in the system.

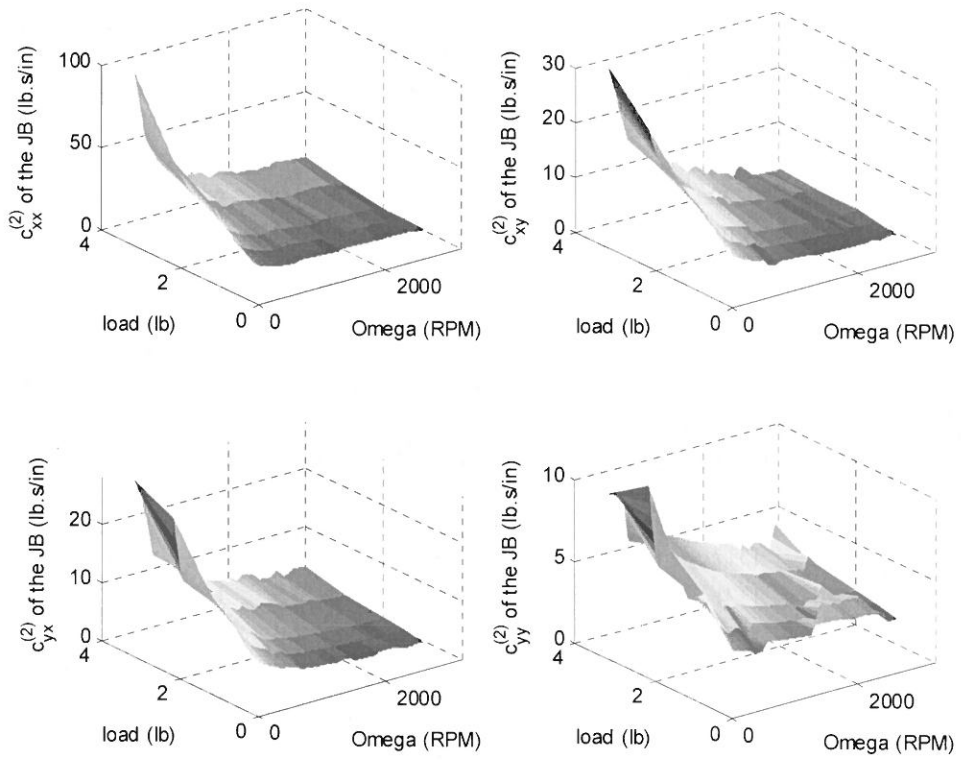

Fig. 12. Estimated journal bearing damping coefficients as a function of load and speed based on the Neural Network Model (Metamodel of the theoretical model).

Comparison between Experimental and Analytical Results

The system response with the estimated parameters (enhanced model) was compared with the original one, and the results are shownfor an input load of 2.316 lb (10.3 N). This load condition was used for estimating the system parameters. Figure 9 represents the relation between the input speed Ω versus the displacement (in y-direction) for rotors B (outboard drive). The enhanced model predicted the rotor bearing system

response better than the original model. Two important remarks can be obtained from Figure 9:

1) The peak vibration amplitude of 0.75 mils for the original model increased to match the experimental values of 1.3 mils; and,

2) The peak vibration which occurs at $\Omega \approx 1650$ rpm for the original model shifted closer to the experimental actual values of $\Omega \approx 1410$ rpm (defined as the 1st critical speed). The first critical speed location here is based on the location of the rotor vibration peak as a function of rotor speed and not on the associated Eigenvalues.

Table 2 outlines the comparisons between the measured and predicted first critical speed values for different static radial load on the mid-span oil-film journal bearing. In this table, the original model had large errors in predicting the correct critical speed location. For all tested static loads, the predicted error of the original model was in the range of 9% - 18%. On the other hand, the enhanced model has a prediction error from 0% - 4%, which is much obviously smaller than the original.

Table 2. Summary of the critical speed at each static load.

	Experimental Results	Simulation without parameter ID. (Original Model)		Simulation with parameter ID. (Enhanced Model)	
Static Load (lb.)	1st Critical speed (rpm)	1st Critical Speed (rpm)	Difference (%)	1st Critical Speed (rpm)	Difference (%)
0.823	1317	1450	9.150%	1317	≈ 0%
1.321	1371	1510	9.205%	1371	≈ 0%
1.817	1312	1570	16.43%	1320	0.61%
2.316	1355	1650	17.86%	1355	3.90%
3.808*	1420	1700	16.47%	1410	0.70%

*Used for model validation only. Not included in the RSM training.

A common trend in proving the generality of the estimated parameters, is testing the model on untrained data at a different load. Figure 13 shows the original and enhanced models compared to the experimental results for an input load equal to 3.808 lb. The results demonstrate that the enhanced model is robust, and it gives better simulation compared to the original. For example, the original model predicts the 1st critical speed at 1700 rpm with a maximum peak response of 0.6 mils which represents 16.47% of the experimental one. Meanwhile, the enhanced model predicts this critical speed at a speed equal to 1410 rpm with a maximum peak value of 1.4 mils which represents only a 0.7% difference.

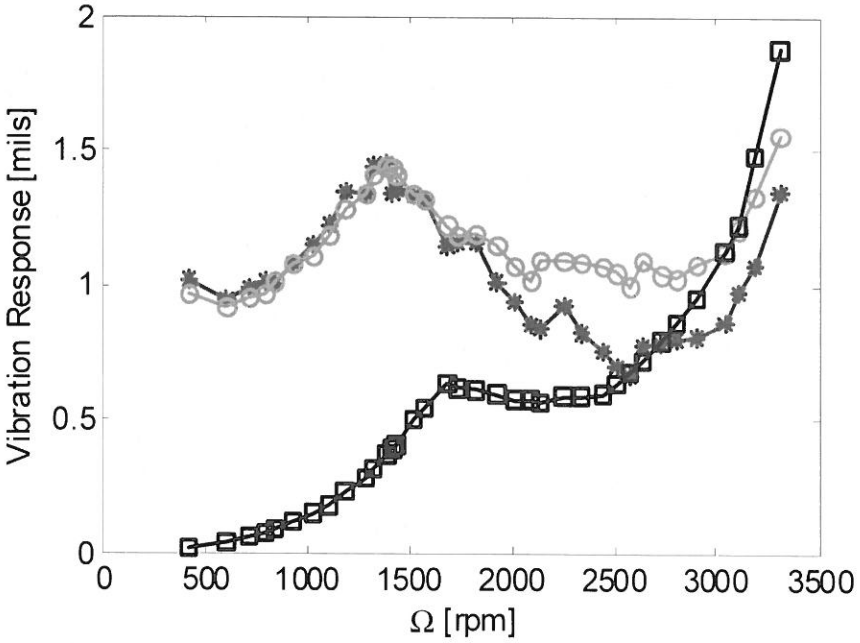

Fig. 13. Rotor vibration synchronous response of disk 2 (displacement) with input load = 17.4 N (3.817 lb) for (—□—) Simulation with system coefficients based on Sommerfeld number. (···*···) Simulation with system coefficients based on parameter estimation. (—○—) Experimental.

As a verification step to show the model improvement for the new system with estimated parameters, the instability threshold speeds were extracted, and the results were excellent. Table 3 shows the comparison of the instability threshold speeds of the experiment, original simulation, and simulation results with estimated parameters. For all tested static loads, the predicted error of the original model was 8.34% - 14.4%. On the other hand, the enhanced model had a prediction error of 2.19% - 4.74%, which is much smaller than the original model.

Table 3. Summary of the instability threshold speed at each static load.

	Experimental Results	Simulation without parameter ID. (Original Model)		Simulation with parameter ID. (Enhanced Model)	
Static Load (lb.)	Instability Threshold (rpm)	Instability Threshold (rpm)	Difference (%)	Instability Threshold (rpm)	Difference (%)
0.823	2838.37	2475	12.8%	2955	3.95%
1.321	2877.71	2480	13.8%	2965	2.94%
1.817	2805.32	2469	12.0%	2945	4.74%
2.316	2919.58	2500	14.4%	2985	2.19%
*3.808	3164.02	2900	8.34%	3100	2.02%

* Used for model validation only. Not included in the RSM training.

For higher static loads, there was still some difference in the result. This may be due to experimental measurements, model assumptions, and/or from the optimization assumption of the lower and upper band of stiffness and damping coefficients measured from non-dimensional parameters.

CONCLUSIONS

In this study, the overall comparisons between experimental results and analytical outputs for the original rotor-bearing model without parameter estimation were not satisfactory. Consistently, the simulation predicted critical speed differed from the experimental results. These consistent differences strongly suggest that the journal bearing coefficients should be estimated as a function of speed and static load. In addition, the journal bearing coefficients were also corrected using the parameter estimation method. An optimization methodology using pattern search techniques was implemented to determine the unknown parameters of the rotor-bearing system. The design space was defined based on the estimated parameters using the Sommerfeld number.

Finally, the enhanced model succeeded in predicting the actual responses of the system with minor differences between the simulated and the actual responses at different loading and speed conditions. This enhanced model creates a great interest in developing smart systems for predictive maintenance and troubleshooting of high performance turbo-machinery that benefit from advanced identification procedures. Moreover, the model can be used for enhancing the performance of rotor bearing systems via optimization methods. More studies could improve design of rotor-bearing systems with minimum power loss, which show unbalance and stress reduction on rotor shafts.

REFERENCES

Adams, M. & Falah, A. 2004. Experiments and modeling of a three-bearing flexible rotor for unbalance response and instability thresholds. Presented at the 8th International Conference on Vibrations In Rotating Machinery, 7-9 September, Swansea, UK.

Adams, M. 2001. Rotating machinery vibration: From analysis to trouble shooting. Marcel Decker, New York.

Andres, L. & Santiago, D. 2005. Identification of journal bearing force coefficient under high dynamic loading centered static operation. Tribology Transactions **48**: 9-17.

Andres, L. & Santiago, O. 2004. Forced response of a squeeze film damper and identification of force coefficients from large orbital motions. ASME Journal of Tribology **126**(2): 292-300.

Assis, E. & Steffen, V. 1999. Multicriterion techniques for the optimization of rotors, in nonlinear dynamics, chaos, control, and their applications to engineering sciences. Vibrations with Measurements and Control 2: 236–249.

Beale, M., Hagan, M. & Demuth, H. 2012. Neural network toolbox user's guide in MATLAB-Version R2012b, Math Works, USA.

Camargo, L., Castro, H. & Cavalca, K. 2010. "Identification of misalignment and unbalance in rotating machinery using multi-objective genetic algorithms". In: *Proceedings of the 8th IFToMM International Conference on Rotordynamics*, Seoul, Korea.

Castro, H. 2013. Comparison in the application of genetic algorithm and particle swarm optimization in unbalance identification in rotating machinery. 22nd International Congress of Mechanical Engineering (COBEM 2013) November 3-7, Ribeirão Preto, SP, Brazil

Charles, A. & Dennis, J. 2004. A pattern search filter method for nonlinear programming without derivatives. SIAM J. Optimization **14**(4): 980–1010.

Chouksey, M., Dutt, J. K. & Modak, S. 2014. Model updating of rotors supported on journal bearings. Mechanism and Machine Theory 71: 52–63.

Cook, R., Malkus, D., Plesha, M. & Witt, R. 2001. Concept and applications of finite element analysis, 4th Edition, Wiley, USA.

Dakel, M., Baguet, S. & Dufour, R. 2014. Nonlinear dynamics of a support-excited flexible rotor with hydrodynamic journal bearings. Journal of Sound and Vibration **333**:2774–2799.

Falah, A. 2002. Modeling and experiments of linear and nonlinear dynamics of a flexible multi-bearing rotor, PhD Thesis, Case Western Reserve University.

Goldberg, D. 1989. Genetic algorithms in search optimization, and machine learning. Addison-Wesley, USA.

Han, F. & Haiyang, Gao, X. 2013. Bearing parameter identification of rotor-bearing system based on kriging surrogate model and evolutionary algorithm. Journal of Sound and Vibration **332**: 2659-2671.

Jiang, G., Hu, H., Jin, Z. & Xie, Y. 1997. Identification of oil film coefficients of large journal bearings on a full scale journal bearing test rig. Tribology International **30**(11): 789-793.

Kostrzewsky, J., Taylor, V. & Flack, D. 1997. Experimental determination of the dynamic characteristics of a two-axial groove journal bearing. Tribology Transactions Journal **37**(3): 534-542.

Lia, W. Jiang, Z., Wanga, T. & Zhuc, T. 2014. Optimization method based on generalized pattern search algorithm to identify bridge parameters indirectly by a passing vehicle. Journal of Sound and Vibration **333**(2): 364-380.

Meruane, & V. Pascual, R. 2008. Identification of nonlinear dynamic coefficients in plain journal bearings. Tribology International **41**: 743-754.

Nicoletti, R. 2013. Optimization of Journal Bearing Profile for Higher Dynamic Stability Limits. Journal of Tribology **135**: 011702-1- 011702-13.

Nordmann, R. & Schollhorn, K. 1981. Identification of stiffness and damping coefficients of journal bearings by means of the impact method. Institution of Mechanical Engineers Conference Vibrations in Rotating Machinery, Cambridge, **C285/80**: 231.

Rosa, L. Magluta, C. & Roitman, N. 1997. Modal parameters estimation using an optimization technique, Proceedings of 15th International Modal Analysis Conference, February 3–6: 540–544.

Sawicki, J. & Rao, T. 2004. A Nonlinear model for prediction of dynamic coefficients in a hydrodynamic journal bearing. international journal of rotating machinery **10**(6): 507–513.

Tieu, A. & Qiu, Z. 1994. Identification of sixteen dynamics coefficients of two journal bearings from experimental unbalance responses. Wear **177**(1): 63-69.

Tiwari, R. & Vyas, N. 1995. Estimation of Non-linear Stiffness Parameters of Rolling Element Bearings from Random Response of Rotor-bearing Systems. Journal of Sound and Vibration 187 (2): 229-239.

Tiwari, R. & Vyas, N. 1997. Non-linear bearing stiffness parameter extraction from random response in flexible rotor-bearing systems. Journal of Sound and Vibration **203**(3): 389-408.

Torczon, V. 1997. On the convergence of pattern search algorithms. SIAM Journal on Optimization 7(1): 1–25.

Yang, T. & Lin, K. 2009. Identification of speed-dependent bearing coefficients from unbalance responses in one test run. ASME Turbo Expo 2009: Power for Land, Sea, and Air, 6: Structures and Dynamics, Parts A and B, Orlando, Florida, USA, June 8–12.

Zengeya, M. & Gadala, M. 2012. Empirically derived optimization model: theoretical formulation and validation. Tribology International **47**: 145–15.

Submitted: 11/9/2013
Revised: 23/3/2014
Accepted: 23/3/2014